JOURNAL OF GEOPHYSICAL RESEARCH, VOL. 102, NO. C7, PAGES 15,567–15,581, JULY 15, 1997

On the unsteady separation/intrusion of the Gaspé Current and variability in Baie des Chaleurs: Modeling studies

Jianping Gan [1] and R. Grant Ingram

Department of Atmospheric and Oceanic Sciences, McGill University, Montreal, Quebec, Canada

Richard J. Greatbatch

Department of Physics and Physical Oceanography, Memorial University of Newfoundland, St. John's, Canada

Abstract. A numerical model has been used to study separation/intrusion of an unsteady, baroclinic coastal jet, the Gaspé Current (GC) and its impact on dynamics and thermodynamics of the Baie des Chaleurs (BdC, Gulf St. Lawrence, Canada). The model has 2 $\frac{1}{2}$ layers with primitive equation dynamics and an embedded bulk mixed layer (ML) model. It is forced with observed atmospheric fluxes, as well as the GC. The simulations show that the variability in the Baie des Chaleurs is controlled by the characteristics of the unsteady GC separation/intrusion. On the basis of the dynamic and vorticity balance analyses, it is found that the separation is related to the adverse pressure gradient force which is induced by the ageostrophic terms in the momentum equations and to local vorticity intensification due to the inertial effect in the flow. The simulations demonstrate characteristics of unsteady separation. The presence of separation in an accelerating current, as well as in a linear current, with strong deceleration when momentum advection is neglected, gives new insight into the mechanisms of unsteady boundary current separation. Unsteady separation or intrusion occurrence depends on the magnitude of the GC transport, as well as its rate and duration of deceleration or acceleration. The GC intrusion generates cyclonic circulation in the BdC. Prevailing westerly winds reduce the cyclonic circulation inside the bay but have little effect on separation/intrusion near the entrance. The GC either intrudes along the coastline (attachment) or after separation (reattachment). Increasing vertical shear of the GC and offshore movement of the GC axis reduces the tendency to separate. The finding of an asymmetric response of GC separation/intrusion to symmetric GC forcing explains the monthly mean features seen in observations taken in the bay.

1. Introduction

Coastal currents encountering a bend in the coastline sometimes leave the coast, overshoot, and form eddies in the interior. On other occasions, the currents turn around the bend and maintain their path along the coast. The nomenclature for the first case is "separated" flow, while in the second case, it is said to be "nonseparated" or in a state of "attachment". For separated flow, the current can also change its path, flow into the interior of the ocean and re-attach to the coast some distance downstream. This phenomenon is called "reattachment".

Earlier studies on the separation problem were mainly based on laboratory experiments dealing with fluid mechanical problems [e.g., *Batchelor,* 1967]. One of the mechanisms described results from the generation of the adverse pressure gradient near the boundary layer [*Schlichting,* 1979; *Tritton,* 1988]. Recently, *Bormans and Garrett* [1989] found that the criterion for separation seems to be $R_w < u/f$, where u is the characteristic flow speed and R_w is the radius of curvature of the exit corner. A modified criterion was later given by *Klinger* [1994a] as $R_w < uW/fR$, where W is the upstream current width and R is the internal Rossby radius. *Klinger* [1994b] also studied the baroclinic eddy generation at a sharp corner in laboratory experiments, which investigated factors affecting separation and corresponding eddy generation. Studies in a two-layer system, by *Ou and Ruijter* [1986], found that a current can loop back on itself due to inertial and beta effects after separation from the coast. *Ou* [1994] also discussed the different

[1]Now at College of Oceanic and Atmospheric Sciences, Oregon State University, Corvallis

Paper number 97JC00589.
0148-0227/97/97JC-00589$09.00

coastal curvature effects on a jet. Numerical experiments with a density current in a strait [*Wang*, 1987] showed the formation of an anticyclonic gyre at the exit of the strait during current separation, which was associated with changes in the Bernoulli potential of the current. *Boudra and Chassignet* [1988] numerically investigated the retroflection and ring formation of the Agulhus Current. They found that retroflection is controlled by the local vorticity balance and noted the importance of the divergent component in this balance. *Haidvogel et al.* [1992] applied a quasi-geostrophic model to the problem of Gulf Stream separation. They found that separation is associated with the occurrence of an adverse value of the high-order pressure gradient. *Smith* [1986] also suggested that an adverse pressure gradient is generated by strong nonlinearity just outside of the boundary layer. *Signell and Geyer* [1991], based on a dynamical analysis, demonstrated that flow separation occurs when the pressure gradient along the boundary switches from favoring to adverse.

Despite the numerous hypotheses that exist, there is no conclusive dynamical explanation available for boundary current separation. In particular, most lack a discussion of unsteady current separation, which is essential in determining the variability in the ocean. The separation/intrusion problem in the Baie des Chaleurs (47.5°-48.5°N, 65.5°-66.5°W, called BdC hereafter; Figure 1) is associated with a time dependent coastal jet, wind stress, thermal forcing, coastal curvature, rotation, and boundary friction factors. The combination of these influences has rarely been dealt with in previous studies.

In this paper, observed variations in the BdC and separation/intrusion characteristics of the unsteady Gaspé Current (GC) are numerically investigated. The main purpose of the paper is to further discuss the observed variability described by *Gan* [1995] using the numerical model. In particular, the nature of seasonal separation/intrusion of the unsteady GC, as well as its effect on the seasonal dynamics and thermodynamics in the BdC, will be discussed. The experiments are also selected to illustrate the factors which affect GC separation/intrusion and oceanographic conditions in BdC.

2. Model Formulation and Implementation

2.1. Model

In this section, the model developed by *Gan et al.* [1995, 1996] will be briefly reviewed. The model consists of two active layers and a deep resting lower layer (Figure 2a). The model equations for momentum, continuity, temperature, and salinity for the upper and lower layers (i=1, 2) are

$$(h_i\mathbf{U_i})_t + \nabla\cdot(h_i\mathbf{U_i}\mathbf{U_i}) + f\mathbf{K}\times h_i\mathbf{U_i} = \delta_{i1}\frac{\tau_0}{\rho_0} - h_i\nabla P_i + (-1)^{i+1}W_e H(W_e)\mathbf{U_2} + H(-W_e)\mathbf{U_1}] + \delta_{i2}W_r\mathbf{V_r} + K_u\nabla\cdot(h_i\nabla\mathbf{U_i}) \quad (1)$$

$$(h_i)_t + \nabla\cdot(h_i\mathbf{U_i}) = (-1)^{i+1}W_e + \delta_{i2}W_r \quad (2)$$

$$(h_iT_i)_t + \nabla\cdot(h_i\mathbf{U_i}T_i) = \frac{Q_i}{\rho_0 C_p} + (-1)^{i+1}W_e[H(W_e)T_e + H(-W_e)T_1] + \delta_{i2}W_rT_r + K_m\nabla\cdot(h_i\nabla T_i) + C_{Ti} + \delta_{i2}N_T \quad (3)$$

$$(h_iS_i)_t + \nabla\cdot(h_i\mathbf{U_i}S_i) = (-1)^{i+1}W_e[H(W_e)S_e + H(-W_e)S_1] + \delta_{i2}W_rS_r + K_m\nabla\cdot(h_i\nabla S_i) + C_{Si} + \delta_{i2}N_S \quad (4)$$

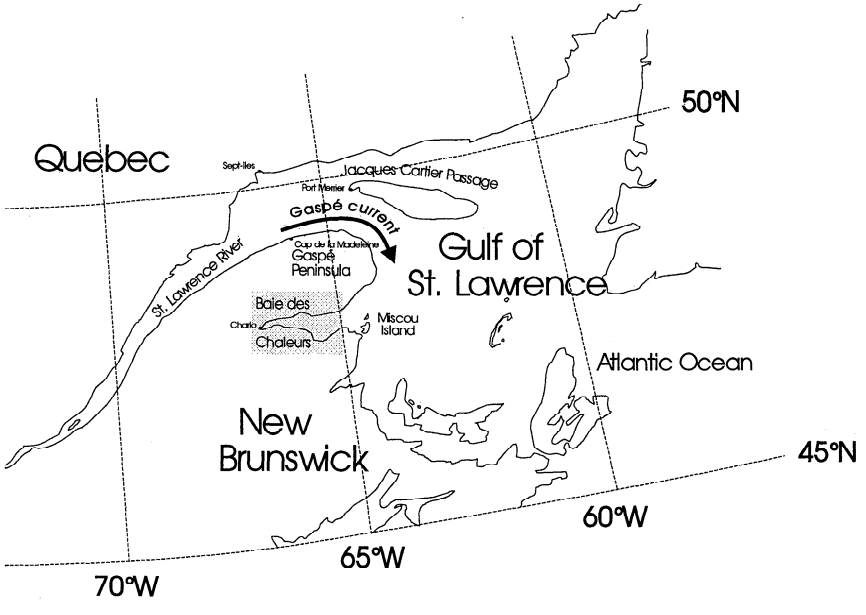

Figure 1. Geographic locations of the Gulf of St. Lawrence and Baie des Chaleurs.

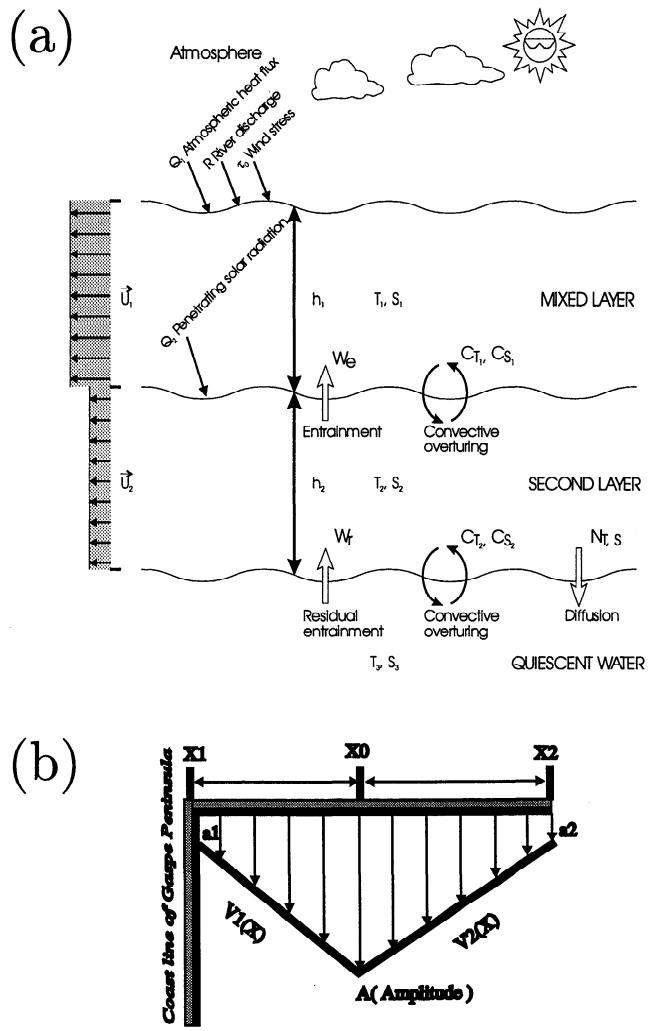

Figure 2. Schematic diagrams of (a) the model and (b) the GC profile applied in the model. In this study, no-slip lateral boundary condition is used (a_1=0).

H is the Heaviside step function and δ_{ik} is the Kronecker delta function. Here τ_0 is wind stress and C_p is specific heat of water. ∇P_1 and ∇P_2 are horizontal pressure gradients in the mixed layer (ML) and subsurface layer, respectively,

$$\nabla P_1 = \nabla(g_1' h_1 + g_2' h_) - h_1 \nabla (g_1'/2) \quad (5)$$

$$\nabla P_2 = \nabla(g_2' h_2/2) + g_2' \nabla (h_1 + h_2/2) \quad (6)$$

where g_1' and g_2' are defined as $g_1'= g(\rho_3-\rho_1)/\rho_0$; $g_2'= g(\rho_3-\rho_2)/\rho_0$; ρ_3 is the density of the deep ocean or lowest layer, which remains spatially constant. Here g is gravity and ρ_0 is a reference density. Density in the model is calculated from the equation of state $\rho=\rho(S,T,Z)$. K_u and K_m are horizontal eddy viscosity and diffusivity coefficients (K_u=40 m^2/s, K_m=30 m^2/s). T_e and S_e are the temperature and salinity at the interface between the ML and the layer below. They are obtained by assuming linear stratification below the ML. The surface heat flux (Q_1) are calculated by observed incoming shortwave radiation, longwave radiation from Berliabd formula, sensible and latent heat given by standard bulk formulations [*Gan,* 1996]. The interfacial temperature flux (Q_2) is determined from penetrating shortwave radiation.

The entrainment and detrainment of the mixed layer are determined from the wind and buoyancy turbulent kinetic energy, as given by *Niiler and Kraus* [1977], but including the effect from shear instability at the base of the mixed layer [*Gan et al.,* 1996]

$$W_e g' h_1 - W_e Ri_{crit}[(u_2-u_1)^2 + (v_2-v_1)^2] = 2m_0 U_*^3 e^{-\frac{h_1}{h_d}} - h_1 m_1 B_0 - \frac{g\alpha h_1 D(h_1) I(0)}{C_p \rho_0} \quad (7)$$

where g'=$g(\rho_2$-$\rho_1)/\rho_0$ and Ri_{crit} is the critical Richardson number between the ML and the subsurface layer below and is set to 0.25. U_*=$(\tau/\rho_1)^{1/2}$ is the friction velocity. The function D(h_1) is given by $D(h_1)$=1-$2h_s/h_1$+$e^{-h_1/h_s}(1$+$2h_s/h_1)$ [*Kim,* 1976]. The buoyancy flux at the base of the ML due to penetrating solar radiation, B_0 can be expressed as

$$B_0 = \frac{g(\alpha Q_1 + \beta Q_R)}{\rho_1 C_p} \quad (8)$$

where m_0 is a mixing efficiency coefficient associated with wind-driven turbulence and m_1 is a coefficient associated with frictional energy dissipation of the convective mixing. Here α and β are the heat and salt expansion coefficients, α=-$(1/\rho_0)(\partial\rho/\partial T)$, β=$(1/\rho_0)$ $(\partial\rho/\partial S)$ and are determined from the equation of state ρ=$\rho(S,T,Z)$. The penetration depth scale (h_d) results from wind-driven turbulent dissipation and is taken as 15 m. We take m_0 equal to 1.2, and m_1 =0.83, if B_0>0 and m_1=1 if B_0< 0. Q_R is equivalent heat flux due to the freshwater flux mainly from precipitation minus evaporation, which was neglected in this study.

W_r in the equations is defined as the residual entrainment rate at the bottom of the second layer *Yuen et al.,* 1992]. It equals zero except when the second layer is shallower than the prescribed depth (H_e=20 m in the model). The model parameterizes the processes of convection (C_{Ti}, C_{Si}) and deep ocean diffusion (N_T, N_S) as well as mass entrainment at the base of the lower layer (W_r) due to strong upwelling or cooling. $\mathbf{V}_r$=0 or =$\mathbf{V}_2$ if W_r>0 or <0 and (T_r,S_r)=(T_3,S_3). Further details about the model and the parameters used are given by *Gan et al.* [1996].

With an internal Rossby radius of about 8 km in BdC, a grid size of $\Delta X \times \Delta Y$=2 km×4 km and an Arakawa C staggered grid were used. The time step t_e was chosen as 10 minute. A modified Orlanski implicit [*Camerlengo and O'Brien,* 1980] type radiation scheme is applied to the upper (h_1) and lower (h_2) layer depth at open boundaries. We put a zero-gradient condition for the alongshore velocity and calculated the component normal to the shore in the same way as in the main program. The condition with zero gradient in layer depth was applied on the northern boundary in order to sup-

press spurious Kelvin wave propagation [*Greatbatch and Otterson,* 1991]. The lateral boundary conditions on the sidewall of the bay are no slip.

2.2. Model Implementation

As indicated by previous investigators [*El-Sabh,* 1976; *Mertz and El-Sabh,* 1989], the GC diverges over the Laurentian Channel and the Magdalen Shallows after leaving the north shore of the Gaspé peninsula. That part of the GC moving along the east coast of the Gaspé peninsula (i.e., the amount entering the northern open boundary in the model domain) is determined as F_a=$F\cos\alpha$, where F is the total GC transport in the ML, estimated on the north shore of the Gaspé peninsula, and α=63° is the estimated angle between the GC and the Gaspé coastline. The GC velocity applied on the northern boundary is assumed as shown in Figure 2b. *Benoit et al.* [1985] found that the position of the maximum GC flow axis varied from nearshore to about 14 km offshore from June to November. This effect is included in the model by changing X_0 in Figure 2b. The GC is applied within 28 km of the coastline. The GC velocity profile in Figure 2b is then determined from its transport as follows. Two linear functions, f_1 and f_2, are assumed to represent the velocity profiles on the two sides of the jet axis, according to the observed lateral profile of the GC from *Benoit et al.* [1985]. Therefore

$$v_1(x) = Af_1(x) = A\left\{\frac{(1-a_1)(x-X_0)}{X_0-X_1}+1\right\} \qquad X_1 \le x \le X_0 \quad (9)$$

$$v_2(x) = Af_2(x) = A\left\{\frac{(1-a_2)(x-X_0)}{X_0-X_2}+1\right\} \qquad X_0 \le x \le X_2 \quad (10)$$

where v_1 and v_2 (Figure 2b) are the southward velocity on the west and east portion of the GC axis, respectively. A is the maximum amplitude of the GC, and a_1=0 (no slip) and a_2=0.3 with

$$v_1(X_1) = a_1A \quad (11)$$

$$v_2(X_2) = a_2A \quad (12)$$

The transport, F_a, is then,

$$F_a = \sum\{v_1(x)h(x)\,\triangle x + v_2(x)h(x)\,\triangle x\} \quad (13)$$

Given F_a, a_1, a_2, X_0 and layer thickness $h(x)$ from model output, A can be determined from (13) by using (9) and (10) and hence v_1, v_2. The velocity entering the northern boundary in the lower layer is calculated using the same method. However, the total transport in the lower layer is kept as F=2.6 x10 ^{4}m^3/s, which corresponds to the observed current strength in the lower layer [*Gan et al.,* 1995].

The study in this paper will be based on atmospheric data obtained during 1990. Since no GC transport observations are available, monthly GC volume transports are chosen so as to be close to those of *Bugden* [1981]. Several typical cases representing possible GC fluctuations are also examined. The GC characteristics and transport for each experiment are summarized in Table 1 and Figure 3, respectively. The BdC is ice covered from mid-December to mid-April. Since coupling with an ice model will not be included in the present study, only the ice-free months will be discussed. The prevailing wind in the BdC was westerlies with very weak N-S component during the study period. The highest air temperature (15 °C) occurred in August. The model is spun up from April to July with observed atmospheric forcing, as well as the GC. The initial temperature and salinity of the model variables are estimated from available data near the bay entrance [*Petrie,* 1990] in April. The temperature and salinity at the open boundaries varied following the seasonal data from *Petrie* [1990]. During the whole integration, monthly mean forcing from both the atmosphere and the GC is linearly interpolated into each time steps.

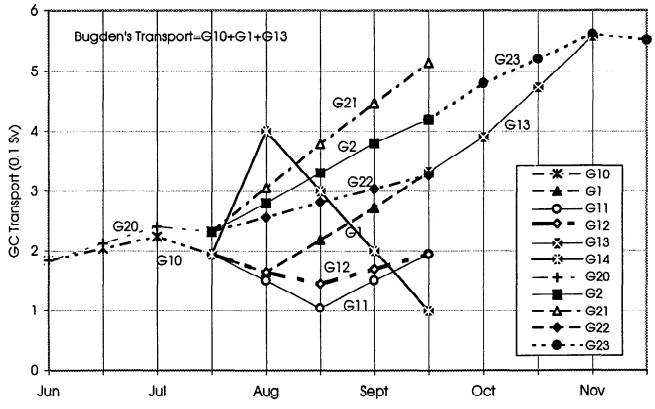

Figure 3. Monthly GC transports of *Bugden* [1981] and GC values applied in experiments. Each unit in the horizontal axis is equal to 15 days and the time for each month is defined in the mid-month. The transports here are values applied to the upper layer of the model. Details are explained further in the text as well as in Table 1.

2.3. Subinertial Variability From Model

In order to make a comparison with the observations [*Gan,* 1995], we first describe higher-frequency variability in the BdC, based on the numerical results obtained using hourly atmospheric forcing, low pass filtered with a 36 hour cutoff.

Figure 4a shows the energy spectra from the model output at Bonaventure for the ML. Kinetic energies in the 10 to 5 day period band have strong amplitudes in association with wind forcing as in observation study. The thermal fields basically respond to the dynamical forcing (not shown). Similar conditions are found at the other stations around the bay [*Gan,* 1995]. Both dynamical and thermodynamic results are very similar to the observations shown in Figure 4b.

3. Separation in a Decelerating/Accelerating GC

Whether the unsteady GC separates or not greatly depends on the characteristics of the GC itself. In this section, the separated and nonseparated GC characteristics are elucidated with the model results forced by a decelerating/accelerating GC. The processes which relate to the mechanisms for the separation/intrusion of the unsteady GC are discussed. The circulation conditions in the BdC corresponding to the characteristics of GC separation are also described.

3.1. Unsteady Separated and Nonseparated GC (Experiment G_1)

In order to match with the observation period discussed by [*Gan*, 1995], model results forced by the climatological GC [*Bugden*, 1981] in August and September will be presented first. As shown in Figure 3, the applied GC transport in experiment G_1 decreases from mid-July toward the minimum value in mid-August and increases thereafter. The model results show that the GC moved southward along the Gaspé coastline and then separated from the coast near the salient edge in August (Figure 5a). In the lee of the separated GC, there is an anticyclonic recirculation. Although the westerly wind stress decreased at the beginning of August [*Gan*, 1995], the westward intrusion current only generated a weak cyclonic circulation in the central part of the bay (Figure 5a). However, both separation and its induced recirculation at the entrance of the bay were strong in August. In September, the GC intruded into the bay along the coastline (Figure 5b). The cyclonic circulation in the bay was intensified and the anticyclonic recirculation at the bay entrance in August was replaced by a cyclonic eddy west of Miscou Island. During this time, the GC transport (F) quickly increased to the values of 2.72 x 10^5 m^3/s and 3.31 x 10^5 m^3/s by the middle and the end of September (Figure 3), respectively. The transition process above can be seen in the time series of the E-W velocity along profile A (Figure 6). It shows that the eastward current on the north shore (north end of profile A, hereafter referred to as region A) and the westward current in the southern part of profile A, respectively, occurred before mid-August when the GC was decelerating. Following GC acceleration, the westward intruding current shifted to the north shore and led to an attachment of the GC (Figure 5b), even though the larger Reynolds number (VL/K_u) was favorable for current separation [*Dengg*, 1993].

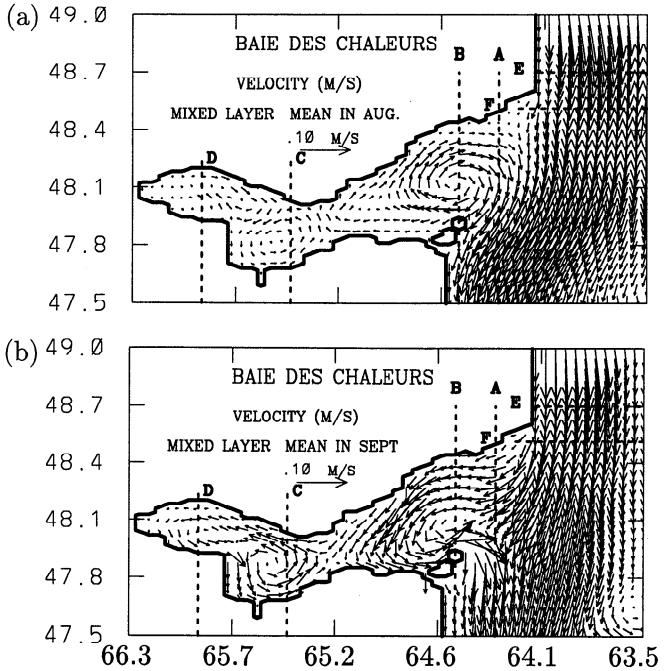

Figure 5. Monthly mean circulation in the mixed layer for case G_1 in (a) August and (b) September. The thick dashed lines show the locations of profiles A, B, C, D, E, and F.

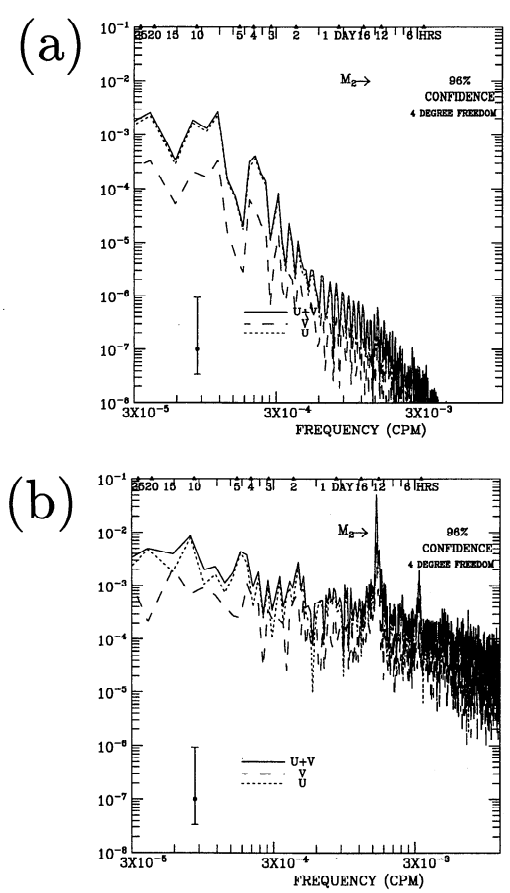

Figure 4. Energy spectra of (a) simulated and (b) observed velocity at station Bonaventure. Ordinate units are u^2/s^2.

3.2. The Adverse Pressure Gradient Force (APGF)

One of the classical approaches in determining separation processes is based on the local dynamical balance related to the pressure gradient force (PGF). This has been extensively discussed by many previous investigators [e.g., *Batchelor*, 1967; *Schlichting*, 1979; *Trit-*

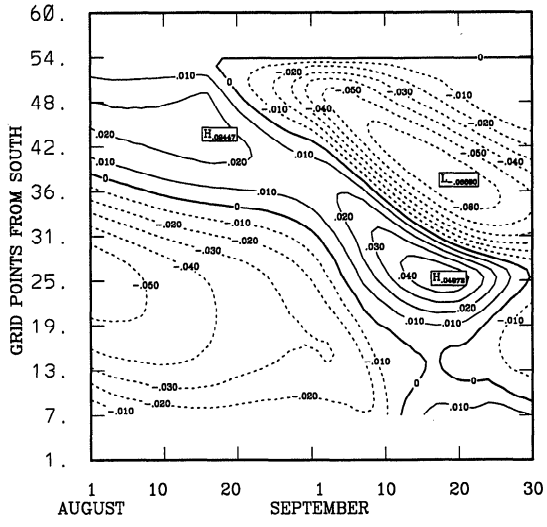

Figure 6. Time series of E-W velocity (m/s) along profile A in G_1. Positive values refer to the eastward currents.

ton, 1988] in the nonrotational plane. In the BdC, the dynamical balance in the flow is mainly dominated by the geostrophic balance as shown in Figure 7. On the other hand, departure from geostrophy can be of vitally important in determining the change in the flow, even though the ageostrophic terms are small. Combined with Figure 6, Figure 7 shows that a net northward ageostrophic PGF (APGF) which opposes the southward GC was generated at the time of a decelerating GC. With (1), the N-S APGF can be written as

$$APGF = -h_1 \frac{\partial P_1}{\partial y} - f h_1 u_1 = (h_1 v_1)_t + \nabla(h_1 v_1 \mathbf{v_1}) - \frac{\tau_y}{\rho_0} - W_e[H(W_e)v_2 + H(-W_e)v_1] - K_u \nabla \cdot (h_1 \nabla v_1) \quad (14)$$

It can be seen that the northward PGF increases when the local acceleration and diffusion terms were positive. The term related to the entrainment is negligible. The numerical results are similar to the finding of *Haidvogel et al.* [1992], that rapid deceleration of boundary currents can generate separation due to an adverse, along-boundary high-order pressure gradient term. We use the term "adverse" in the sense that the PGF is against the southward GC along the Gaspé coastline. It should be noted that in the classical boundary layer separation, the adverse pressure gradient is associated with a spatially decelerating flow that is steady in time [*Batchelor*, 1967]. *Smith* [1986] has suggested that the adverse pressure gradient can be generated by strong nonlinearity just outside the boundary in the steady case. Close to the boundary, however, the nonlinear terms are small compared to the other terms during the separation due to the deceleration of GC, as shown in Figure 7. The fact that separation/attachment coincides with the time of GC deceleration/acceleration indicates that the unsteady GC can also strengthen/weaken the spatially change of the flow as compared with steady flow. *Signell and Geyer* [1991] found that the recirculation formed in a unsteady flow is stronger than the one formed in steady flow due

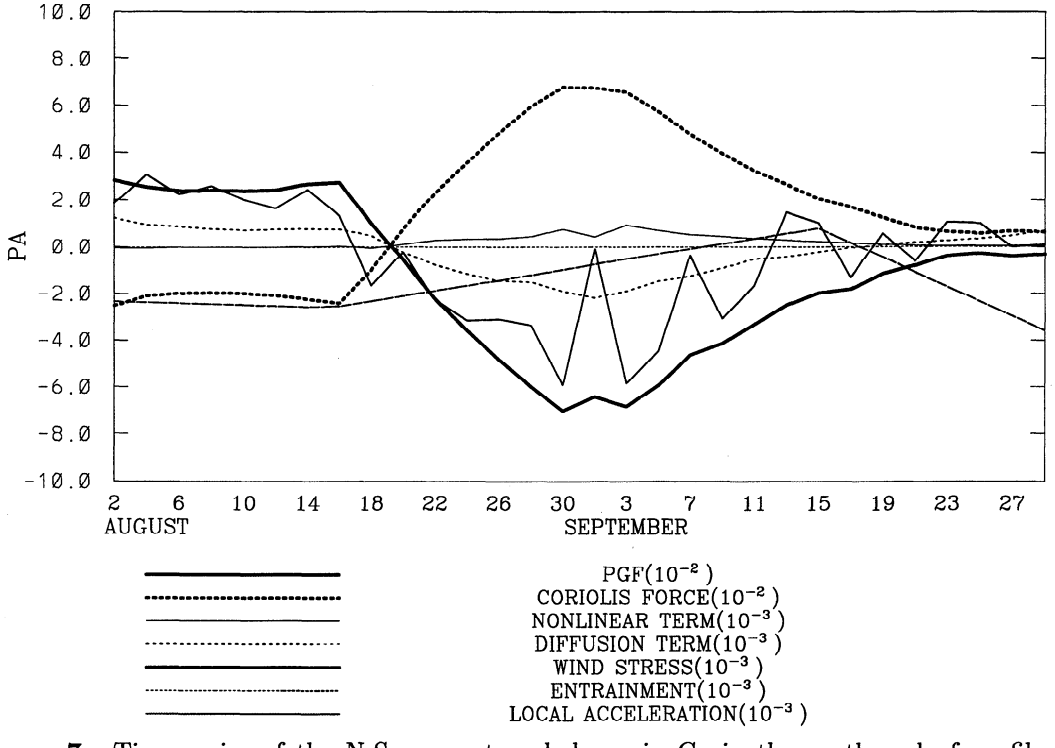

Figure 7. Time series of the N-S momentum balance in G_1 in the north end of profile A. PGF, $-h_1\rho_0\partial P_1/\partial y$; Coriolis force, $-fh_1u_1\rho_0$; nonlinear term, $\rho_0\nabla(h_1v_1\mathbf{v}_1)$; diffusion term, $-\rho_0K_u\nabla\cdot(h_1\nabla v_1)$; wind stress, $-\tau_y$; entrainment term, $-W_e[H(W_e)v_2+H(-W_e)v_1]\rho_0$. Positive value refers to the northward direction.

to intensification of vorticity during the formation process. In our experiments with a steady GC [e.g., *Gan et al.*, 1995], the separation strength was much weaker than in the case described here with unsteady GC, as was the adverse PGF. It is important to point out that an adverse PGF is a necessary but not a sufficient condition to support separation. The survival of the separation also depends on the adverse vorticity which is controlled by the local vorticity balance (e.g., counterbalancing diffusion and/or advection, etc.), as indicated by *Tritton* [1988]. Further elucidation of the separation process will be discussed in the following sections in combination with the numerical results.

3.3. Separation and Vorticity Field

An alternative approach to investigate the separation process is to analyze the vorticity of the flow. Figure 8a shows that when separation occurred in the decelerating GC on day 10, a positive vorticity was generated near region A. Therefore the oncoming flow from upstream was not able to pass close to the coastline. To the south, negative vorticity formed a vortex (see also Figure 5a) and reinforced the adverse PGF to the north of the vortex. During attachment, when the GC accelerated on day 46 (Figure 8b), negative vorticity was advected into the bay along the north shore, and the existing positive vorticity in region A was transported southward. It cut off the eastward current near the north shore as well as the separation of the GC. The time evolution of vorticity near the entrance is shown in Figure 9. Similar to the eastward current in Figure 6, positive vorticity near region A is quickly advected southward, away from the north shore and replaced by negative vorticity when the GC started to accelerate in mid-August.

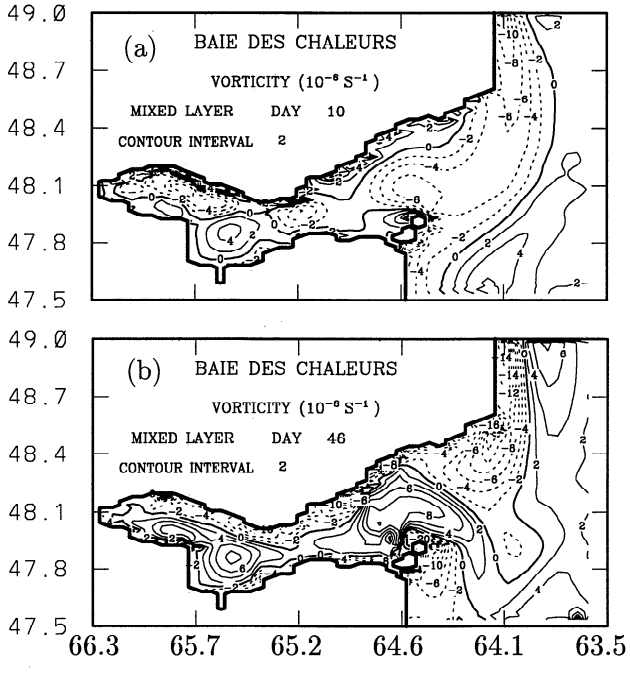

Figure 8. Horizontal distribution of vorticity (a) on August 10 (separated) and (b) on September 15 (nonseparated) in G_1, respectively.

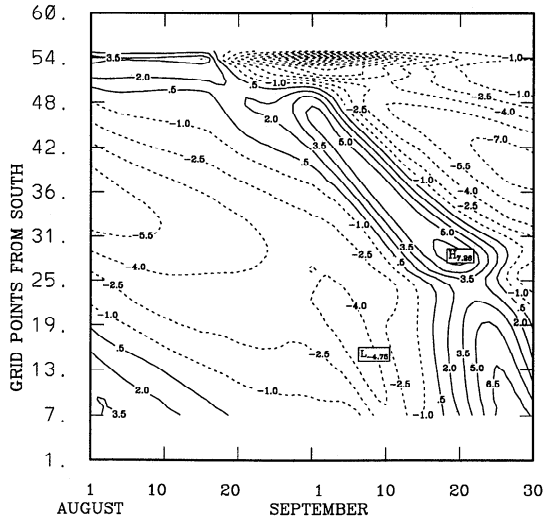

Figure 9. Time series of vorticity (10^{-6} s^{-1}) along profile A in G_1.

The sources of the negative vorticity are either advection from the Gaspé coastline upstream or local generation between the westward coastal current and the no-slip boundary. *Ou* [1994] found that only with an accelerating jet does the strong flow extend to the coastal boundary, where the viscous shear layer is confined. Therefore negative vorticity advected downstream along the Gaspé coastline during GC acceleration was able to shed the positive vorticity off the boundary layer near the region A. As the positive vorticity was advected southward and replaced the previous negative vorticity in the recirculation region at the entrance (Figure 8b), the separation was cut off.

Another vorticity source may be from centrifugal upwelling induced by coastline curvature [*Cherniawsky and LeBlond*, 1986]. The rising of the interface would be accompanied by negative vorticity near the salient edge [*Wang*, 1987], which tends to reinforce recirculation and separation. The results of our unsteady boundary current modeling show that negative vorticity induced by this manner is at least 1 order of magnitude less than the advection term.

3.4. GC Intrusion and Its Effect on the Circulation in BdC

As favorable conditions to separation disappear, the flow is able to attach to the northern coastline as it intrudes into the bay (Figure 5b), which then strengthens the cyclonic circulation inside the bay. In August, the intrusive current in the separated GC associated with the westward current in the recirculation results in a very weak cyclonic eddy in the bay center. In fact, most of the intrusion from the recirculation (due to separation) in August returns to the Gulf of St. Lawrence by the eastward flow in the recirculation. For the case of nonseparated GC in September (G_1), the continuously attached GC is able to penetrate deeply into the bay and generated much stronger eddies inside the BdC (Figures 5b and 8b).

Table 1. Summary of Experiments

Case	Descriptions
G_1	Bugden's GC in August and September
(G_{11}, G_{12})	(GC with higher and lower decelerating rates)
(G_{14})	(nonlinearity and pressure gradient force experiment)
G_2	stronger GC in August and September
(G_{21}, G_{22})	(GC with higher and lower accelerating rates)
G_{23}	October and November
G_3	effect of vertical shear in GC (August-September)
G_4	larger GC offshore distance (August-September)
G_5	symmetric and asymmetric separation (August-September)

Previous studies have tended to relate the strength of the circulation inside the BdC directly to the strength of the GC. In reality, the relation between the GC (and its separation) and the intensity of the cyclonic circulation inside the BdC is far more complicated. This is investigated in two cases (G_{11} and G_{12}; Figure 3 and Table 1). The results show that a higher GC deceleration rate but a weaker volume transport in G_{11} (as compared with G_{12}) gave a stronger separation. It intensified the anticyclonic recirculation at the entrance but weakened the cyclonic eddy inside the bay, even though the intrusive current was as strong as the weaker separation case, G_{12}. Therefore it can be concluded that for a decelerating GC, the separation intensity of the GC was positively correlated with its deceleration rate, while the cyclonic eddy inside the BdC was enhanced when the GC strength was strong and its deceleration rate small. The results also imply that a strong GC may not be able to generate a strong cyclonic circulation inside the BdC. The findings agree with the observations (July 1991) discussed by *Gan* [1995].

The prevailing westerly wind stress can also provide anticyclonic vorticity and prevent the formation of the cyclonic eddies in the bay. It was found that when the westerly wind stress was reduced by 80%, it strengthened the cyclonic eddies in the central and western parts of the bay but changed the circulation only slightly near the entrance. This suggests that the wind stress mainly affects cyclonic circulation inside the bay and has little influence on the separation/intrusion characteristics near the bay entrance.

3.5. Inertial Separation in an Accelerating GC (G_2)

In experiment G_2 (shown in Figure 3 and Table 1), a stronger GC in August and September, as well as earlier acceleration starting from the beginning of August, is adopted. A slightly stronger GC is also used in June and July (G_{20}). Results obtained here are much different from those in G_1. The velocity of southward moving GC along profiles E and F increased by about 5 cm/s, as compared with G_1. In contrast to G_1, the flow in August was able to intrude along the north shore, even though most of the GC moved southward (Figure 10a). The eddies in the center and west of the BdC were strengthened as compared with that in G_1. In September, separation and recirculation were (surprisingly) formed in contrast to the attachment in G_1 (Figure 10b), although the GC was accelerating in both cases. The phenomena will be discussed based on the vorticity balance.

As the GC accelerated from the beginning of August, separation should have ceased, for reasons explained in the last section. The current intruded along the north shore. The positive vorticity in region A which remained from the decelerating GC after mid-July (Figure 3), was replaced by a negative vorticity at the beginning of August (Figure 11a). The horizontal vorticity distribution (not shown) was similar to Figure 8b in G_1 when

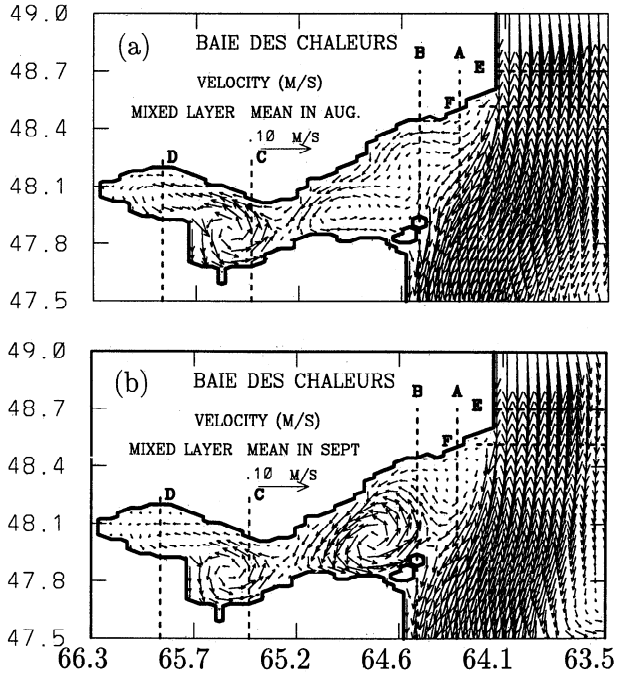

Figure 10. Monthly mean circulation in the mixed layer of G_2 in (a) August and (b) September. The current speed in the figure is truncated at 0.1 m/s.

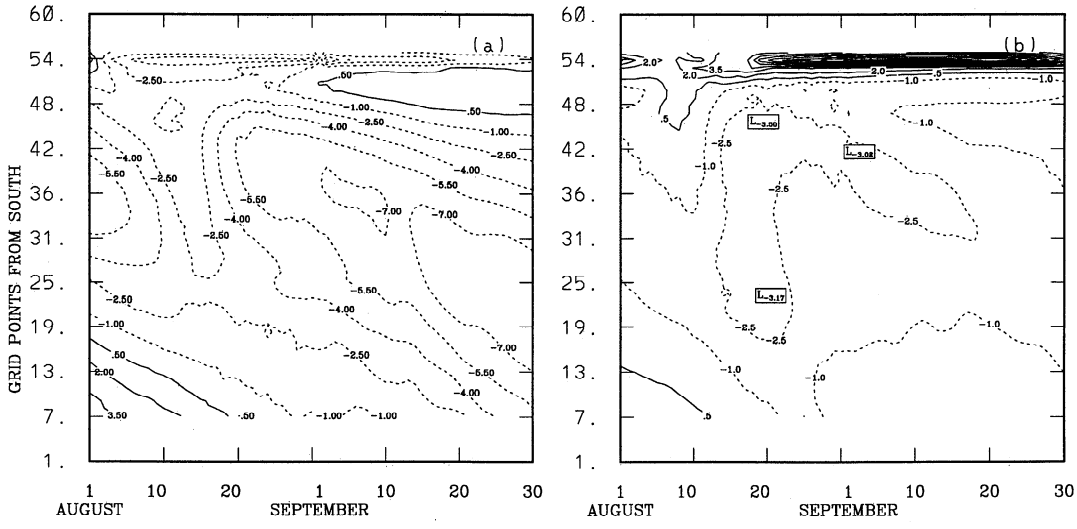

Figure 11. Time series of vorticity at (a) upper and (b) lower layers along profile A in G_2.

the GC did not separate. However, when the GC further accelerated in September, the cyclonic eddy west of Miscou Island intensified and extended northward to the north shore (Figure 12a). This led to an positive vorticity at the beginning of September (and an eastward current) near region A (Figure 11a) in association with separation.

The separation found for an accelerating Gaspé Current in September, in contrast to the nonseparation for the accelerating GC in G_1, was, in fact, generated by

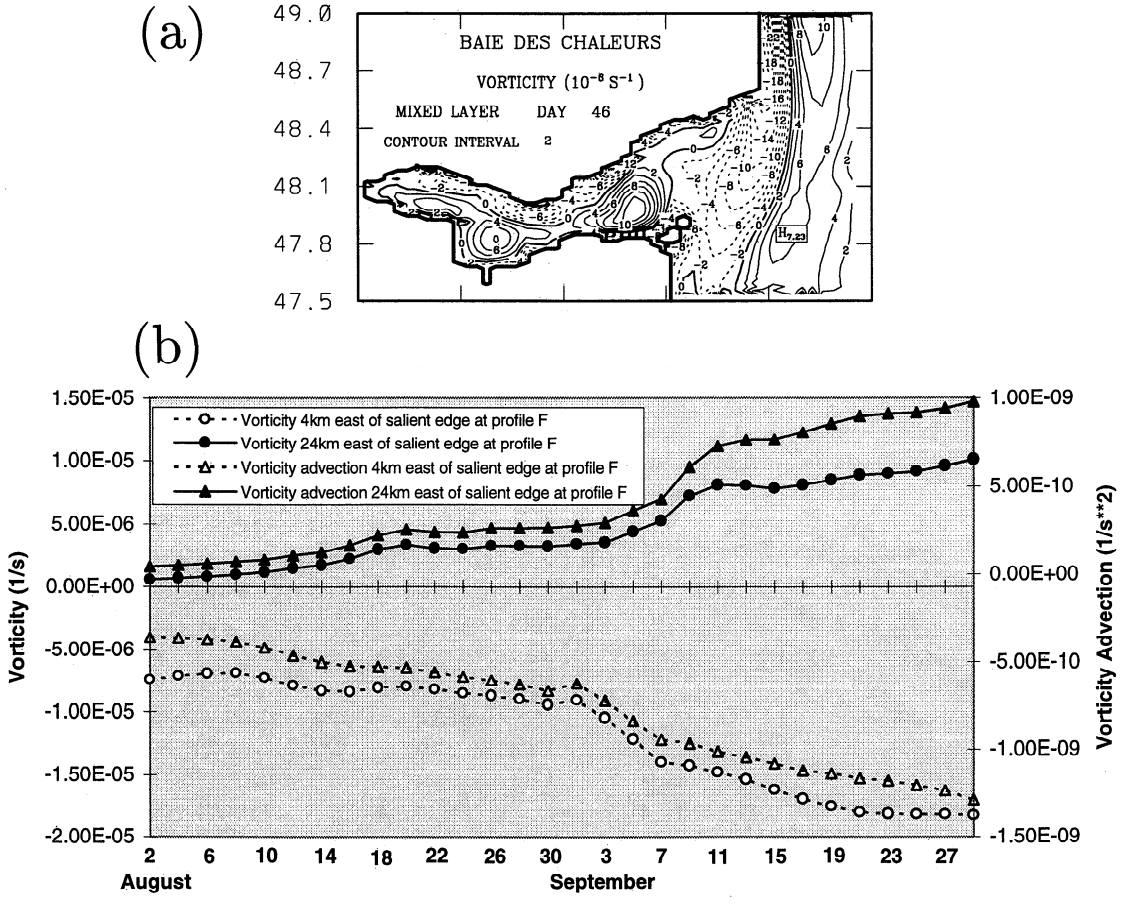

Figure 12. (a) Horizontal distribution of vorticity for G_2 on September 15 (b) Time series of the vorticity and vorticity advection downstream of salient edge. The GC axis was located 15 km east of salient edge.

increasing nonlinearity in the GC. As shown by previous investigators [e.g., *Werner et al.*, 1988; *Gan et al.*, 1996], nonlinearity in the boundary current can play a major role in generating separation. In terms of vorticity balance, the inertial effect resulted in downstream advection of strong negative vorticity, which was generated between the no-slip Gaspé coast and the southward GC and diffused into the whole boundary current [*Dengg*, 1993]. More negative vorticity accumulated downstream when the GC accelerated to a large value, forming a recirculation near the bay entrance. The eastward current associated with the northern recirculation in turn induced a positive vorticity near the boundary layer in region A and hence separation.

Figure 12b confirms that both vorticity and its advection quickly increased on both sides of the GC axis, as the GC separated at the beginning of September. Unlike a coarse-resolution model, which has much larger eddy viscosity to parameterize sub-grid-scale turbulence, vorticity diffusion is relatively weak in our eddy-resolving model. The viscous stress curl term in the vorticity equation is at least 1 order of magnitude less than the advection term in G_2. Thus the vorticity change is mainly controlled by vorticity advection, as illustrated by Figure 12b. Therefore the GC separated mainly due to the inertial effect of the current, when enough negative vorticity accumulated downstream to generate the recirculation.

It is interesting to note that in the lower layer, vorticity in region A had a sign opposite to that in the ML (Figure 11b). The positive vorticity is associated with separation even though there was no separation in the ML.

On the basis of the discussion above, it can be concluded that although the acceleration of the GC could reduce the northward PGF, the strong negative vorticity advected southward by the intensified GC was able to generate a recirculation and separation. These findings extend our understanding of the separation mechanism in terms of the importance of the inertial effects and the vorticity field.

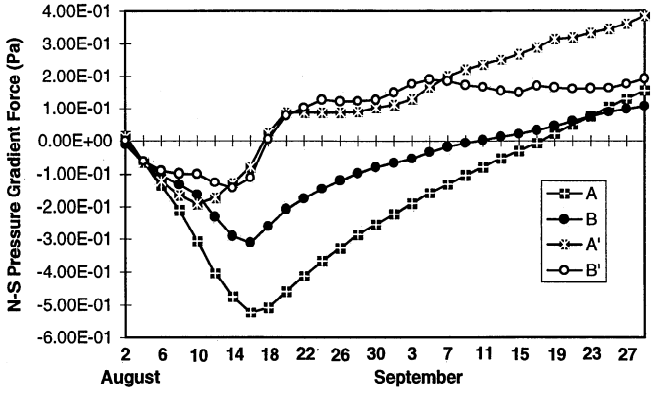

Figure 13. Time series of PGF calculated 4 km offshore for profiles A and B for case G_{14}. A and B (A' and B') refer to the case without (with) inclusion of the momentum advection terms. Positive value refers to the northward (adverse) pressure gradient force.

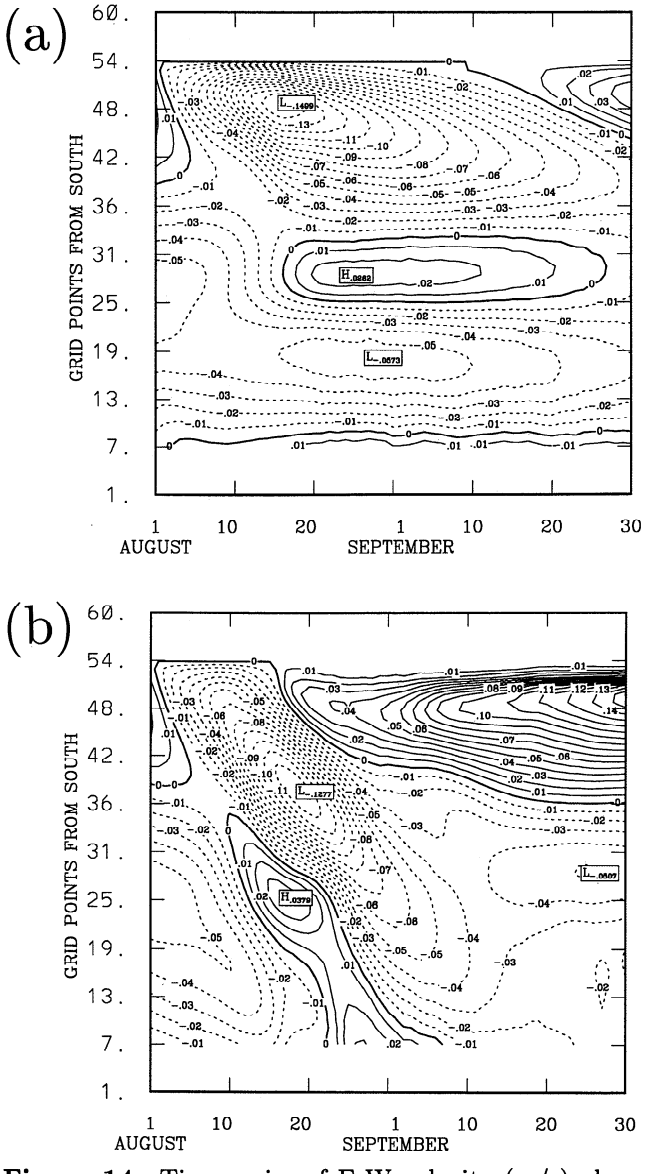

Figure 14. Time series of E-W velocity (m/s) along profile A in G_{14} (a) without and (b) with inclusion of the momentum advection terms. Positive values refer to the eastward currents.

3.6. Some Features of Unsteady Separation

With strong nonlinearity and a weak adverse PGF, the characteristics of separation associated with an accelerating GC in G_2 were quite different from that associated with a decelerating GC in G_1. To distinguish the physical processes at work, an experiment without inclusion of the momentum advection terms together with an unsteady GC was undertaken. The experiment, G_{14} (Figure 3 and Table 1), illustrates that dropping the nonlinear terms in the momentum equations significantly weakened the separation in a decelerating GC. A much weaker separation was generated without inclusion of the momentum advection terms, and separation occurred about 1 month after the GC started to decelerate (Figures 13 and 14a). In contrast, with inclusion of the momentum advection terms, the sepa-

ration was quickly generated as the GC decelerated in mid-August, and the separation occurs almost immediately after the onset of GC deceleration (Figures 13 and 14b). The results suggest that the generation of separation is strongly related to the nonlinear processes at work. Nevertheless, a linear GC with strong deceleration can also generate separation. As mentioned in our previous study [*Gan et al.*, 1996] and by *Werner et al.* [1988], the steady GC will not separate without inclusion of nonlinear terms in the momentum equations. The results here indicate the different separation characteristics in steady and unsteady boundary currents. The separation in the linear case may be due to the positive diffussion and local acceleration. If both nonlinear and diffusion terms are neglected, separation is not generated, both for a steady or unsteady GC. Furthermore, there was no separation in an accelerating GC (e.g., G_2) without inclusion of the momentum advection terms, which further confirms the dominant role of inertial terms for separation associated with an accelerating GC.

We also ran the experiment with 1.5 (G_{21}) and 0.75 (G_{22}) times the GC acceleration rate in G_2 (Figure 3, Table 1), to identify the relation between the inertial separation and characteristics of the GC. The results in G_{21} show that the GC separation occurs within a shorter accelerating period, as compared with G_2. The case with a weaker GC acceleration rate (G_{22}) was also able to generate separation, after a longer time of acceleration (about 1 month after G_{21}). It is noteworthy that the GC strength in G_{22} was smaller than that in G_{21} at the time of the separation. This fact suggests that inertial separation depends not only on the strength of the flow nonlinearity but also on the duration of the flow acceleration which is probably due to the process of vorticity accumulation.

3.7. Characteristics Related to Separation/Intrusion in the BdC

The pre-existing circulation of G_2 near the entrance in August had a separated pattern similar to that in G_1 (Figure 5a), which remained from the strongly decelerating GC in July (Figure 3). When the GC accelerated in August, an opposite circulation pattern generated a weaker (monthly mean) circulation near the bay entrance (Figure 10a). These results agree with previous findings from observations [*Gan*, 1995] concerning the influence of a pre-existing circulation pattern.

In September of G_2, part of the separated GC reattached to the north shore, turned westward, and reinforced the cyclonic eddy near the entrance (Figure 10b). The intensified separation, however, gradually reduced the strength of the intrusive current (Figure 15) and the cyclonic eddies inside the bay toward the end of September as the GC further increased in strength. Thus, even though the GC was stronger, separation reduced cyclonic circulation in the bay [*Gan*, 1995].

In experiment G_2, temperature fronts formed at the entrance of the bay, as the result of the thermal contrast between the bay and the GSL (not shown). River runoff from the west end of the bay and intruding saltier water from the GSL also generates a salinity front at the center of the bay. The temperature in the ML reached a maximum value in August, corresponding to the time of the highest air temperature in 1990.

4. Results With an Intensified GC in Late Fall (G_{23})

The period chosen for this run is between October and November 1990. The transport values of the GC are indicated to be the same as G_{23} in Figure 3, following G_2. As compared to September, mean cyclonic eddies in the bay were weaker in October and nearly disappeared in November (Figure 16), as the GC transport further increased (i.e., GC was accelerating). A very deep ML occurred in the GSL region and was associated with the strong GC and atmospheric cooling during this season. A stronger GC led to a larger inertial radius of the current and greater negative vorticity being advected across the entrance of the bay. With a continuously intensifying GC from August to late fall, the recirculation eddy was elongated in the lee of the GC, near the entrance. It detached the cyclonic eddy west of Miscou Island from the main flow of the separated GC. The intensified separation of the GC gradually weakened the westward intrusion current from the bifurcation of the reattachment and almost cut it off in November.

It should also be noted that the westerly wind stress was much stronger in both October and November than earlier in fall and summer [*Gan*, 1995]. This could also limit westward GC intrusion. To distinguish effects of intensified westerly wind stress and stronger GC separation on the weakening of the cyclonic circulation inside the bay for this season, a run with wind stress reduced by 80% was conducted. It was found that even with a

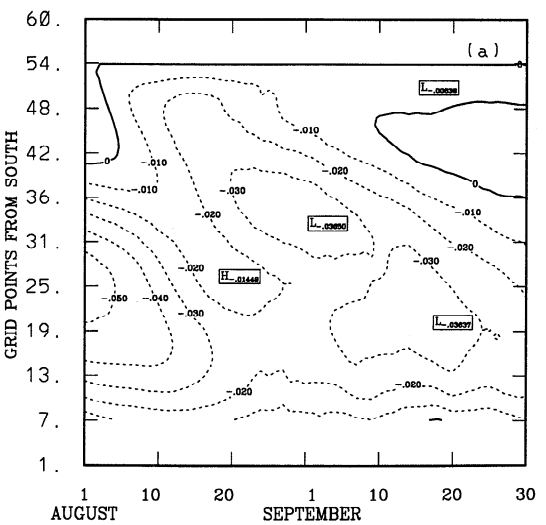

Figure 15. Time series of E-W velocity (m/s) (and strength of the corresponding eddies) for profile A of G_2. The bay entrance is located between grid points number 25 and 55 in profile A.

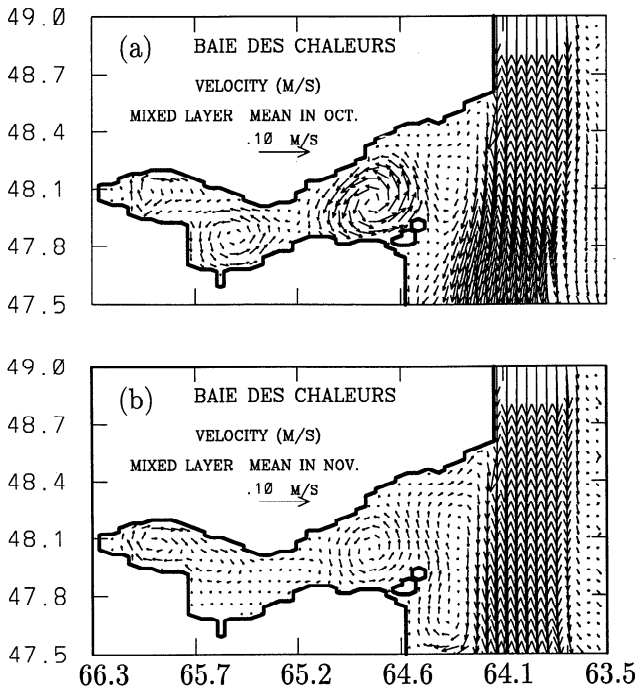

Figure 16. Monthly mean circulation and layer thickness in the mixed layer of G_{23} in (a) October and (b) November. The current speed in the figure is truncated at 0.1 m/s.

much weaker westerly wind stress ($\tau'_{x,y}=0.2\tau_{x,y}$), the cyclonic circulation in the bay increased only slightly [*Gan*, 1995]. It can then be concluded that although the intensified westerly wind stress can reduce cyclonic circulation, the weakening of the cyclonic circulation in G_{23} is due to mainly the intensification of the GC separation and the weaker intrusive current.

The width of the GC applied at the northern boundary was kept constant in experiment G_{23}. However, the internal Rossby radius, $R_D=\sqrt{g'h_1h_2/(h_1+h_2)}$, was reduced from 5 km in the warm (August) to 3 km in colder (November) period. It narrowed the width of the GC downstream. This finding verifies what *Benoit et al.* [1985] had found from observation. The narrower GC width also led to intensification of the GC in the ML.

ML deepening occurred in this season as the air temperature dropped rapidly, which extended the GC in the vertical. A strongly separated GC advected cold and salty water southward and formed a thermal front between the GC and the GSL (not shown). This thermal front also deterred intrusion of the GC into the bay, as the buoyancy forcing diverted the GC southward.

5. Effect of the Gaspé Current Structure on Separation/Intrusion

In this section, the effect of changing the GC profile upstream (Figure 2b) on the separation/intrusion will be discussed. The experiments are based on the approach taken in experiment G_2 except that the transport at the lower layer in G_3 and the GC profiles in G_4 are modified.

5.1. Effect of Vertical Shear in the GC (G_3)

In previous experiments, the GC transport in the lower layer was kept at a constant value of 2.6 x 10^4 m^3/s. In this experiment, it is linearly decreased from this value on August 1 to -1.5 x 10^4 m^3/s on August 15 and then kept constant for the rest of the integration.

Stronger shear instability at the base of the ML increases entrainment and incorporates momentum opposite to that of the GC from the lower layer into the ML. Since the GC transport in the ML was kept the same as in G_2, the GC velocity was slowed down as compared to that in G_2, especially in September, when the vertical shear was greater. A weaker GC also led to a decrease in upstream negative vorticity in the boundary layer. Therefore a smaller inertial radius of the current and weaker vorticity advection (as compared to G_2) cut off the separation. Both the GC intrusion (Figure 17a versus Figure 15) and cyclonic eddies in the bay were intensified [*Gan*, 1995].

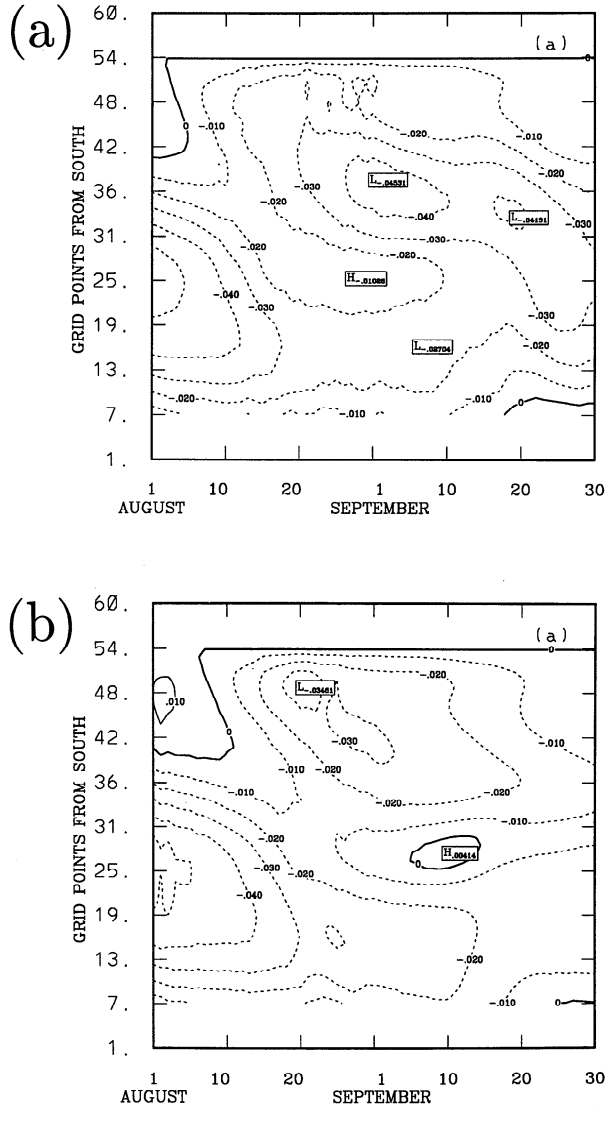

Figure 17. Time series of E-W velocity (m/s) along profiles A and B for (a) G_3 and (b) G_4.

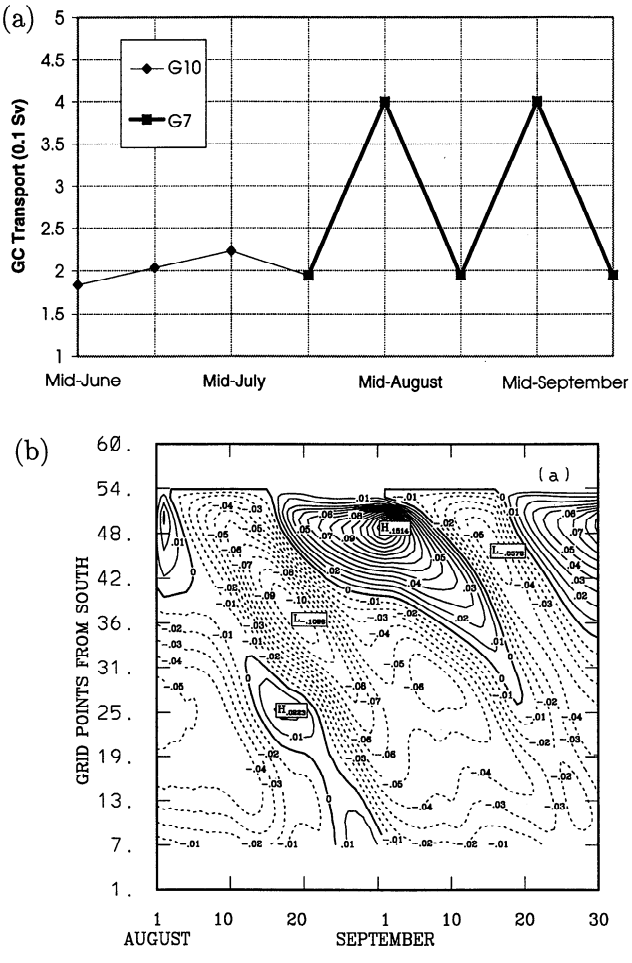

Figure 18. (a) Symmetric GC transport in experiment G_5 and (b) time series of E-W velocity (m /s) along profile A in experiment G_5. Positive values refer to the eastward current.

5.2. Offshore Movement of the GC (G_4)

To examine the effect of offshore movement of the GC axis, as found by *Benoit et al.* [1985], we keep X_0 fixed at 24 km in (9) and (10) (also see Figure 2b). The effect is to weaken the negative vorticity between the GC and the no-slip boundary due to a weaker near shore velocity. Thus only a very weak negative vorticity was advected downstream. The adverse velocity in region A (Figure 17b versus Figure 15) and hence separation were weakened. The cyclonic eddy near profile B was intensified and had a larger horizontal extension.

It should be noted that the values defining the GC profiles in the above experiments (G_3 and G_4) were chosen only to test the sensitivity in August and September and are not necessarily realistic scenarios.

6. Symmetric GC and Its Asymmetric Separation/Intrusion (G_5)

In experiment G_1, the mean circulation in August was dominated by the separated pattern, even though the accelerating GC with the same mean rate of ($|dF/dt|$) as in the early part of the month shifted the circulation to a nonseparated configuration after mid-August. In order to further investigate the effect of GC variation on the separation/intrusion, an experiment with steady wind stress, atmospheric heat fluxes, and periodic GC forcing was run (Figure 18a).

Before mid-August, the accelerating GC intruded into the BdC along the north shore (Figure 18b) and formed a cyclonic circulation west of Miscou Island, similar to that for G_1 (shown in Figure 5b). As the GC decelerated in mid-August, it quickly separated and formed recirculation similar to Figure 5a near the entrance. Figure 19a shows the mean circulation in August averaged from both separated and non-separated circulation pattern in the month. Both cyclonic and anticyclonic circulation appear west and east of Miscou Island, respectively. Due to the two different phases of the GC (i.e., separation and attachment) in August, the mean circulation is the sum of two "unequal" states. The associated mean currents averaged from the opposing direction currents in region A have a weak eastward mean current in the northern part of the recirculation. As compared with the case in August for G_1 (Figure 5a), one finds that the stronger GC here is able to generate a cyclonic eddy west of Miscou Island.

Although the attachment of the current near the north shore was re-established as the GC accelerated in September, the eastward current offshore of profile A, associated with separation in August, remained until September (Figure 18b). In contrast to this slower transition from separated to nonseparated state, the following deceleration of the GC in mid-September led to a quicker cutoff of the intrusive current north of profile A. Thus the monthly averaged westward intrusive current was weaker in September. The mean circulation pattern therefore was dominated by the separated case with much stronger recirculation and weaker cyclonic eddies east and west of the Miscou Island (Figure 19).

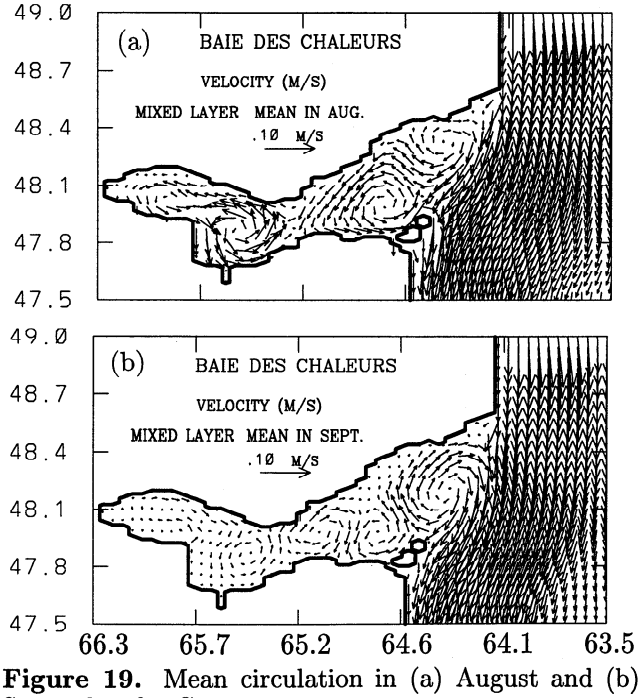

Figure 19. Mean circulation in (a) August and (b) September for G_5.

The above results suggest that a symmetric GC variation does not have a corresponding symmetric response in its separation/intrusion and that the separated current has stronger energy than the nonseparated case. This explains the results in August of experiment G_1 as mentioned at the beginning of this section (Figure 5a). A circulation pattern similar to Figure 19 with an anticyclonic recirculation and a cyclonic eddy to the east and west of Miscou Island, respectively, was also found by *Whitehead* [1985] in a laboratory study of the deflection of a baroclinic jet by a wall. He found that much more fluid flows to the right than to the left after reattachment, which is similar to the above finding. The recirculation was stronger than the cyclonic eddy west of it. The observed circulation has similar features, as discussed by *Gan* [1995].

7. Summary and Conclusions

A 2 $\frac{1}{2}$ layer model with primitive equation dynamics and mixed layer physics has been applied to the BdC to study the observed characteristics of dynamic and thermodynamic variability. The mechanisms of separation/intrusion induced by the remote coastal jet (the Gaspé Current) and the effect of separation/intrusion on the bay have been discussed.

The model results indicate that the cyclonic circulation pattern in the bay is the result of the westward GC intrusion. This pattern prevailed in summer and was greatly reduced in late fall. The seasonal variability inside the bay is mainly determined by the characteristics of separation/intrusion near the entrance of the bay.

To understand the variability in the BdC, one must first be able to describe the separation/intrusion characteristics of the unsteady GC coastal jet. The separation occurrence is related to the adverse pressure gradient force near of the salient edge, which accompanied an eastward current and positive vorticity. The analysis shows that the reverse APGF is induced by the ageostrophic terms in the momentum equations. If the GC is decelerating, separation is mainly induced by the adverse PGF due to the retarding influence of the GC. A stationary anticyclonic recirculation near the entrance of the bay is generated. When the GC accelerates, the separation is cut off. Nevertheless, it is found that the GC can separate during acceleration, if a large negative vorticity advection from upstream is able to form anticyclonic recirculation and induce an adverse PGF in the boundary layer. Although the separation depends critically on including momentum advection terms, a linear GC (the momentum advection terms dropped) with strong deceleration can also generate separation due to the gradual intensification of the diffusion effect. The separation/intrusion of the unsteady GC was found to be controlled by the magnitude of the GC volume transport as well as its phase (accelerating or decelerating), duration, and strength of its deceleration (acceleration).

The GC can intrude into the bay either along the north shore without separation (attachment) or as a westward current in the recirculation after separation (reattachment). A stronger attachment enhances the cyclonic eddies inside the bay. Increasing intrusion by reattachment during the decelerating phase of the GC enhances the eddies inside the bay only when the GC is strong and its deceleration rate was small (G_{11}, G_{12}). When strong inertial effects dominate late fall, strong southward currents and powerful negative vorticity advection finally detach the recirculation from the cyclonic eddy west of Miscou Island and cut off intrusion and reattachment from the southern recirculation.

An increase of vertical velocity shear in the GC enhances the instability at the base of the ML, weakening the separation. Offshore movement of the GC axis reduced its separation but enhanced the cyclonic eddy near the entrance.

It should be mentioned that the theory of unsteady separated flow still requires much to be done, and the results in this paper only highlight some of the characteristics. In conclusion, variability in the BdC results from a complex forcing system and is mainly controlled by separation/intrusion characteristics of the remote unsteady GC coastal jet.

Acknowledgments. We would like to thank to T. Warn for helpful discussions and L. A. Mysak and M. El-Sabh for reviewing the manuscript. Thanks also to Alan Schwartz and J. C. Croteau for computing help. This work was supported by and is a contribution to the program of the Groupe Interuniversitaire de Recherche Oceanographiques du Quebec and OPEN (National Center of Excellence in Canada). Funds were also obtained from the Natural Science and Engineering Research Council of Canada (R.G.I and R.J.G) and the Fonds FCAR (R.G.I).

References

Batchelor, G.K., *An Introduction to Fluid Dynamics*, 615 pp. Cambridge Univ. Press, New York, 1967.

Benoit, J., M. I. El-Sabh, and C. L. Tang, Structure and seasonal characteristics of the Gaspe Current, *J. Geophys. Res.*, *90*, 3225-3236, 1985.

Bormans, M., and C. Garrett, A simple criterion for gyre formation by the surface outflow from a strait, with application to the Alboran Sea, *J. Geophys. Res.*, *94*, 12,637-12,644, 1989.

Boudra, D. B., and E. P. Chassignet, Dynamics of Agulhas retroflection and ring formation in a numerical model,I, The vorticity balance. *J. Phys. Oceanogr.*, *18*, 180-303, 1988.

Bugden, G. L., Salt and heat budgets for the Gulf of St. Lawrence, *Can. J. Fish. Aquat. Sci.*, *38*, 1153-1167, 1981.

Camerlengo, A. L., and J. J. O'Brien, Open boundary conditions in rotating fluids, *J. Comput. Phys.*, *35*, 12-35, 1980.

Cherniawsky, J. Y., and P. H. LeBlond, Rotating flows along indented coastlines, *J. Fluid Mech.*, *169*, 379-407, 1986.

Dengg, J., The problem of Gulf Stream Separation: A barotropic approach. *J. Phys. Oceanogr.*, *23*, 2183-2199, 1993.

El-Sabh, M.I., Surface circulation patterns in the Gulf of St.Lawrence. *J. Fish. Res. Board Can.*, *33*,124-138, 1976.

Gan, J. P., Upper ocean modeling in Baie des Chaleurs, Ph.D thesis, 160 pp, Dept. of Atmos. and Oceanic Sci., McGill Univ., Montreal, Quebec, Canada, 1995.

Gan, J. P, R. G. Ingram, R. J. Greatbatch and P. Chen,

Upper ocean modelling in a coastal bay. *J. Geophys. Res., 100*, 15,977-15,997, 1995.

Gan, J. P, R. G. Ingram, and R. J. Greatbatch, Sensitivity study of upper ocean model in a coastal bay, *J. Mar. Syst., 7*, 203-219, 1996.

Greatbatch, R. J., and T. Otterson, On the formulation of open boundary conditions at the mouth of a bay, *J. Geophys. Res., 96*, 18,431-18,445, 1991.

Haidvogel, A. B, J. C. McWilliams, and P. R. Gent, Boundary current separation in an quasigeostrophic eddy-resolving ocean circulation model. *J. Phys. Oceanogr., 22*, 882-902, 1992.

Kim, J.-W., A generalized bulk model of the ocean mixed layer. *J. Phys. Oceanogr., 6*, 686- 695, 1976.

Klinger, B. A., Baroclinic eddy generation at a sharp corner in a rotating system, *J. Geophys. Res., 99*, 12,515-12,535, 1994a.

Klinger, B. A., Inviscid current separation from round capes, *J. Phys. Oceanogr., 24*, 1805-1811, 1994b.

Mertz, G., and M I. El-Sabh, An autumn instability event in the Gaspe Current, *J. Phys. Oceanogr., 19*, 148-156, 1989.

Niiler, P. P. and E. B. Kraus, One-dimensional models of the upper ocean, in *Modelling and Prediction of the Upper Layers of the Ocean*, edited by E. B. Kraus, pp. 143-172, Pergamon, Tarrytown, 1977.

Ou, H. W., Flow near a continental boundary driven by an oceanic jet, *J. Phys. Oceanogr., 24*, 966-978 , 1994.

Ou, H. W. and W. P. M Ruijter, Separation of an inertial boundary current from a curv ed coastline, *J. Phys. Oceanogr., 16*, 280-289, 1986.

Petrie, B., Monthly means of temperature, salinity and sigma-t for Gulf of St. Lawrence, *Can. Tech. Rep. Hydrogr. and Ocean Sci., 126*, 137 pp., 1990.

Schlichting, H., *Boundary layer theory*, 7th ed., 817 pp., McGraw-Hill, New York, 1979.

Signell, R. P., and W. R. Geyer, Transient eddy formation around headlands. *J. Geophys. Res., 96*, 2561-2575, 1991.

Smith, F., Steady and unsteady boundary-layer separation, *Annu. Rev. Fluid Mech., 18*,197-220, 1986.

Tritton, D. J., *Physical Fluid Dynamics*, 2nd ed., 519 pp., Oxford Univ. Press, New York, 1988.

Wang, D. P., The straits surface outflow, *J. Geophys. Res., 92*, 10,807-10,825, 1987.

Werner, F. E., A. Cantos-Figuerola, and G. Parrilla, A sensitivity study of reduced-gravity channel flows with application to the Alboran Sea, *J. Phys. Oceanogr., 18*, 373-383, 1988.

Whitehead, J. A., The deflection of a baroclinic jet by a wall in a rotating fluid, *J. Fluid Mech., 157*, 79-93, 1985.

Yuen, C. W., J. Y. Cherniawsky, C. A. Lin, and L. A. Mysak, An upper ocean general circulation model for climate studies: Global simulation with seasonal cycle, *Clim. Dyn., 7*, 1-18, 1992.

J. P. Gan, College of Oceanic and Atmospheric Sciences, Oregon State University, 104 Ocean Admin Building, Corvallis, OR 97331-5503. (e-mail: gan@oce.orst.edu)

R. J. Greatbatch,Department of Physics and Physical Oceanography, Memorial University of Newfoundland, St. John's, Newfoundland, Canada, A1B 3X7. (e-mail: rgreat@crosby.physics.mun.ca)

R. G. Ingram, Department of Atmospheric and Oceanic Sciences, McGill Univer sity, Montreal, Quebec, Canada, H3A 2K6. (e-mail: grant@bathybius.meteo.mcgill.ca)

(Received March 27, 1995; revised December 17, 1996; accepted January 3, 1997.)